Journal of Alloys and Compounds 526 (2012) 91–97

Contents lists available at SciVerse ScienceDirect

Journal of Alloys and Compounds

journal homepage: www.elsevier.com/locate/jallcom

Dielectric relaxation behavior of $A_xCo_{1-x}Fe_2O_4$ (A = Zn, Mg) mixed ferrites

Kavita Verma, Ashwini Kumar, Dinesh Varshney*

School of Physics, Vigyan Bhawan, Devi Ahilya University, Khandwa Road Campus, Indore 452001, India

ARTICLE INFO

Article history:
Received 19 December 2011
Received in revised form 10 February 2012
Accepted 13 February 2012
Available online xxx

Keywords:
Chemical synthesis
X-ray diffraction
Scanning electron microscopy
Dielectric response

ABSTRACT

Samples of $A_xCo_{1-x}Fe_2O_4$ (A = Zn, Mg; x = 0.0, 0.5) ferrite were synthesized by chemical co-precipitation method. Room temperature Rietveld – refined X-ray diffraction pattern elucidate the formation of single-phase cubic structure with *Fd*3*m* space group for all prepared samples. Slight variation in the lattice parameter of Mg doped $CoFe_2O_4$ has been observed when compared with $CoFe_2O_4$ and $Zn_{0.5}Co_{0.5}Fe_2O_4$. The variation of permittivity and ac conductivity as a function of frequency reveals that dispersion in all these ferrites is attributed to Maxwell–Wagner type of interfacial polarization. The minimum value of loss tangent (~0.04) at 5 kHz makes $A_xCo_{1-x}Fe_2O_4$ most suitable material for microwave application. Temperature dependent dielectric constant and loss tangent of all the three samples shows an increasing trend with increase in temperature. The activation energy (E_a) for $CoFe_2O_4$, $Co_{0.5}Mg_{0.5}Fe_2O_4$ and $Co_{0.5}Zn_{0.5}Fe_2O_4$ were found to be 0.81 eV, 0.76 eV and 0.63 eV respectively. The electrical modulus study clearly reveals the presence of non-Debye type of dielectric relaxation in the present material.

1. Introduction

Spinel ferrites are magnetic materials with a general formula $(M_{1-x}Fe_x)[Fe_{2-x}M_x]O_4$, the round and square brackets denote the tetrahedral (A) and octahedral (B) interstitial sites. M is the divalent (Mn^{2+}, Fe^{2+}, Co^{2+}, Ni^{2+}, Zn^{2+}, *etc.*) and Fe is the trivalent (Fe^{3+}) metal cation occupying the FCC lattice formed by O^{2-} anions. The magnetic properties of a spinel are sensitive to the types of cation and their distribution amongst the two interstitial sites of spinel lattice [1]. The cation distribution between *A*-site and *B*-site depends on the ionic radii, the type of bonding and the preparation method. Changing the variables as temperature, pressure, magnetocrystalline anisotropy, and composition of metal ions may influence the cation distribution. Ferrites with spinel structure have attracted considerable interest due to their remarkable optical, mechanical, thermal, and magnetic properties that are exploited in many technological applications such as ferrofluid, biomedicine, targeted drug delivery, magnetic resonance imaging, and recording media [2–4].

Apart from the magnetic properties, studies of electric and dielectric behavior are equally important from both fundamental and applied point of view. Polycrystalline ferrites are very good dielectric materials and have many technological applications ranging from microwave to radio frequencies. The high permeability and low electrical conductivity in such materials are very useful for inductor, transformer cores and in switch mode power supplies. The order of magnitude of conductivity greatly influences the dielectric and magnetic behavior of ferrites and is mostly dependent on the preparation method and sintering condition [5]. It has been reported earlier that ferrites sintered in air are highly characterized by conducting grains separated by poorly conducting grain boundaries [6].

Several researchers have incorporated various substitutions and studied the magnetic and dielectric properties of ferrites. For Cu substituted $Ni_{0.5-x}Zn_{0.3}Mg_{0.2}Fe_2O_4$ ferrites, it is observed that the electrical properties such as dielectric constant and loss tangent ($\tan\delta$) decreases with increasing frequency [7]. Usually, the electrical and dielectric properties are mostly controlled by grain boundaries; however, the ferrites have shown to exhibit interesting electrical and dielectric properties in nano form as compared to the bulk counterpart. The dielectric loss of nanocrystalline $NiFe_2O_4$ is two order of magnitude smaller than bulk $NiFe_2O_4$ [8]. Moreover the dielectric permittivity of Ni—Zn ferrite prepared by citrate precursor method are one to two order of magnitude less as compared to that produced by conventional ceramic method [9,10]. Furthermore, the electrical conductivity and dielectric loss decreases with a reduction of grain size in nano structured $ZnFe_2O_4$ [11].

Apart from Nickel ferrite, cobalt ferrite is also treated as a good magnetic as well as dielectric material. It was reported that the dielectric constant increases with increasing calcination temperature of $CoFe_2O_4$ synthesized by chemical auto combustion route method [12]. Moreover the dielectric constant and dielectric loss is found to reduced significantly due to substitution of La^{3+} ion in $CoFe_2O_4$, whereas the DC resistivity was found to be 30 times more as compared to pure $CoFe_2O_4$ [13]. The DC resistivity measurement

* Corresponding author. Tel.: +91 731 2467028; fax: +91 731 2465689.
E-mail addresses: vdinesh33@rediffmail.com, vdinesh33@gmail.com (D. Varshney).

0925-8388/$ – see front matter © 2012 Elsevier B.V. All rights reserved.
doi:10.1016/j.jallcom.2012.02.089

of Ni doped $CoFe_2O_4$ synthesized by co-precipitation method indicates a semiconducting behavior, whereas frequency dependence dielectric constant shows the usual dispersion behavior [14]. Also the dielectric loss of Al^{3+}substituted $CoFe_2O_4$ was found to decrease with Al^{3+} ion concentration [15].

However, no reports have been found in the literature on structural, dielectric feature and impedance spectroscopy of mixed Mg—Co and Zn—Co ferrites. With these motivations we aimed at understanding structural and electrical properties of Mg and Zn doped $CoFe_2O_4$. As per the best of our knowledge, researchers had tried to investigate, analyze, and understand the anomalous properties (*i.e.* structural, electrical, dielectric *etc.*) of ferrites using different experimental technique but an adequate explanation of dielectric properties of doped ferrites is still lacking and offers further investigations. In the present work, we synthesized the doped cobalt ferrites following co-precipitation method, tailoring the structural and electrical properties of Mg and Zn doped $CoFe_2O_4$ using X-ray powder diffraction, dielectric spectroscopy and impedance spectroscopy technique.

2. Experimental details

For the synthesis of $A_xCo_{1-x}Fe_2O_4$ (A = Zn, Mg and x = 0.0, 0.5) samples through chemical co-precipitation technique all the reagents were commercial products with analytical grade without further purification. The chemical reagents for this experiment $Fe(NO_3)_3{\cdot}9H_2O$, $Co(NO_3)_2{\cdot}6H_2O$, $Zn(NO_3)_2{\cdot}6H_2O$, $Mg(NO_3)_2{\cdot}6H_2O$, and sodium hydroxide were used. The water used in all the experiments was distilled with lower conductivity. The aqueous solution of Co, Zn, Fe and Mg salts were freshly prepared by taking $Fe(NO_3)_3{\cdot}9H_2O$, $Co(NO_3)_2{\cdot}6H_2O$, $Zn(NO_3)_2{\cdot}6H_2O$, and $Mg(NO_3)_2{\cdot}6H_2O$ in appropriate molar ratio. This mixture was heated until the temperature reached 70 °C. On vigorous stirring, the pH of the above solution was raised to 12 rapidly, by the addition of 6 M NaOH. The particles settled at the bottom were collected and the top water layer with excess salts was discarded. The particles have been washed repeatedly with distilled water to remove salt impurities. Later, the water washed particles were treated with acetone dried at room temperature and further calcined at 700 °C for 5 h. The samples were pressed into circular disc shaped pellets with a dimension of 1.0 mm thick and 15 mm wide and were further sintered at 1250 °C for 24 h.

The crystal structure and type of phases were identified by means of X-ray powder diffraction (XRD) at room temperature, using Bruker D8 Advance X-ray diffractometer with Cu $K\alpha_1$ (1.5406 Å) radiation. The data was collected with a scanning speed of 2° per minute with a step size of 0.02° over the angular range 2θ ($10° < 2\theta < 80°$) generating X-ray by 40 kV and 40 mA power settings. Microstructure and surface morphology of the samples have examined by scanning electron microscope [SEM: JEOL-JSM-6390]. Frequency dependent dielectric measurements of the present samples were evaluated with impedance analyzer model-Novo control tech Germany alpha ATB works over the wide range of frequency (3 μHz–20 MHz) and in the ac voltage range (100 mV–3 V). The dielectric constant (ε') and loss tangent ($\tan\delta$) were measured as a function of temperature (room temperature to 673 K) in air atmosphere using a Hewlett Packard 4192A (Berkshire, U.K.) impedance analyzer. For dielectric measurements sintered pellets were polished with zero grain emery paper, and coated with high purity silver paste on adjacent faces as electrodes and then dried for 2 h at 150 °C to make the parallel plate capacitor geometry.

3. Results and discussion

3.1. Structural analysis

The X-ray powder diffraction pattern for $A_xCo_{1-x}Fe_2O_4$ (A = Zn, Mg and x = 0.0, 0.5) samples is shown in Fig. 1. From the X-ray diffraction pattern, it has been observed that all the reflection peaks of pure as well as doped compound matches well with Joint Committee for Powder Diffraction Set (JCPDS) Card No. 22 - 1086. Furthermore, there is no change in peak positions for all the three samples, which indicate that all the samples crystallize in single-phase cubic structure with *Fd*3*m* space group. The crystallite sizes of the synthesized samples were determined from the X-ray diffraction data using Debye–Scherrer formalism:

$$t = \frac{0.9\lambda}{\beta \cos\theta} \quad (1)$$

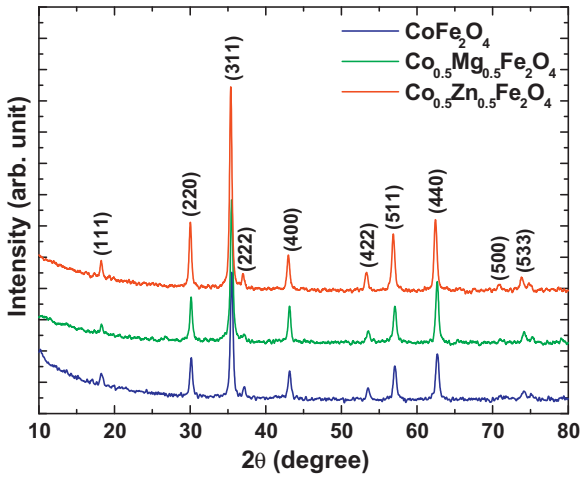

Fig. 1. X-ray powder diffraction pattern for $A_xCo_{1-x}Fe_2O_4$ (A = Zn, Mg and x = 0.0, 0.5) samples.

where t is the crystallite size, β is the full width half maximum (FWHM) of the most intense peak (3 1 1) measured in radians, λ is the X-ray wavelength of the Cu $K\alpha_1$ (1.5406 Å)and θ is the Bragg's angle in Eq. (1). The crystallite sizes are estimated as 41.5 nm, 45.9 nm and 45.0 nm for $CoFe_2O_4$, $Co_{0.5}Mg_{0.5}Fe_2O_4$ and $Co_{0.5}Zn_{0.5}Fe_2O_4$ respectively.

The Rietveld refinement of XRD pattern for all the three samples at room temperature were performed with FULLPROF program and are shown in Fig. 2. The XRD pattern for the *Fd*3*m* structural modal reproduce adequately all the observed reflections and gave practically identical reliability factor. There is a good agreement between observed and calculated pattern using the Rietveld

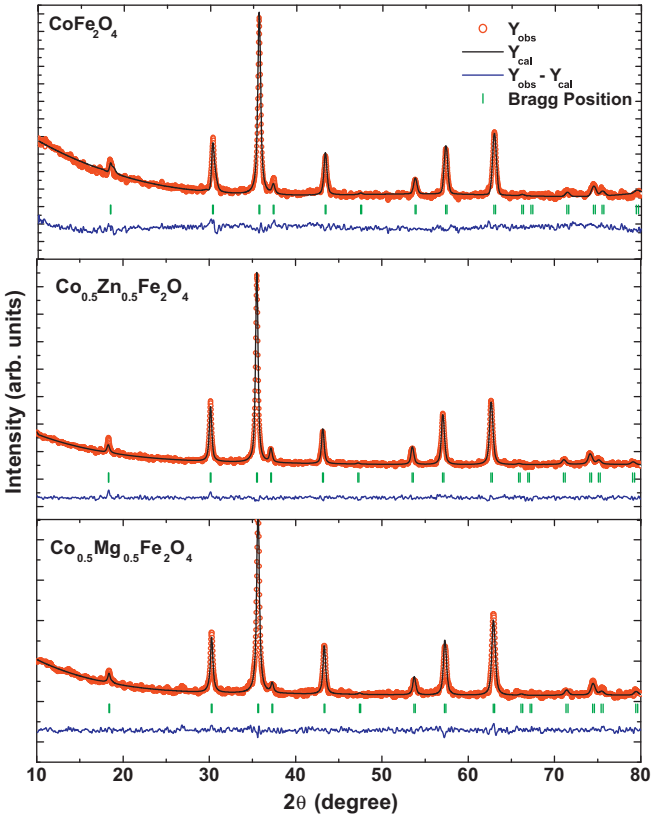

Fig. 2. The observed, calculated, and difference Rietveld refined XRD pattern of $A_xCo_{1-x}Fe_2O_4$ (A = Zn, Mg and x = 0.0, 0.5) samples.

Table 1
Rietveld refined XRD parameters of as synthesized samples.

Samples	$CoFe_2O_4$	$Co_{0.5}Zn_{0.5}Fe_2O_4$	$Co_{0.5}Mg_{0.5}Fe_2O_4$
Space group	*Fd3m*	*Fd3m*	*Fd3m*
Cell parameters (Å)			
a	8.3554	8.3532	8.3221
Cell volume (Å^3)	583.31	582.85	576.36
Atomic positions			
Fe_1/Zn, Mg			
x	0.000	0.000	0.000
y	0.000	0.000	0.000
z	0.000	0.000	0.000
Fe_2/Co			
x	0.625	0.625	0.625
y	0.625	0.625	0.625
z	0.625	0.625	0.625
O			
x	0.247	0.247	0.247
y	0.247	0.247	0.247
z	0.247	0.247	0.247
R-factors (%)			
R_p (%)	43.9	25.4	30.1
R_{wp} (%)	24.3	17.3	22.5
R_{exp} (%)	23.1	16.0	21.2
R_{Bragg} (%)	5.72	4.25	5.60
R_F (%)	5.47	4.10	5.77
χ^2	1.10	1.16	1.19
GOF-index	1.0	1.1	1.2

analysis, which is confirmed by observing the difference pattern. The refined parameters of as synthesized samples are summarized in Table 1. We identify the residuals for the weighted pattern R_{wp}, the pattern R_p, Braggs factor R_{Bragg}, structure factor R_F, and goodness of fit χ^2. Refined occupation cationic positions suggest that all the structures have completely different compositions corresponding to the chemical formula of the compound. The value of χ^2 comes out to be ~1, which may be considered to be very good for estimations. The lattice constant as calculated from Rietveld refinement of $CoFe_2O_4$ and $Co_{0.5}Zn_{0.5}Fe_2O_4$ matches well with each other due to similar ionic radii of Co^{2+} (0.74 Å) and Zn^{2+} (0.74 Å) [16]. However, the lattice constant of $Co_{0.5}Mg_{0.5}Fe_2O_4$ is slightly less as compared to $CoFe_2O_4$, and is attributed to smaller ionic radii of Mg^{2+}(0.72 Å).

In order to understand the morphology and grain shape of as synthesized samples, scanning electron microscopy (SEM) study was carried out. Fig. 3 represents the SEM images of pure and doped ferrite samples sintered at 1250 °C for 24 h. From the micrograph it is clear that sintered samples results in greater densification with less porosity. The average grain size was 3.2 μm for $CoFe_2O_4$. The grain size increases with doping concentration and was found to be 4.7 μm and 7.4 μm for $Co_{0.5}Zn_{0.5}Fe_2O_4$ and $Co_{0.5}Mg_{0.5}Fe_2O_4$ respectively.

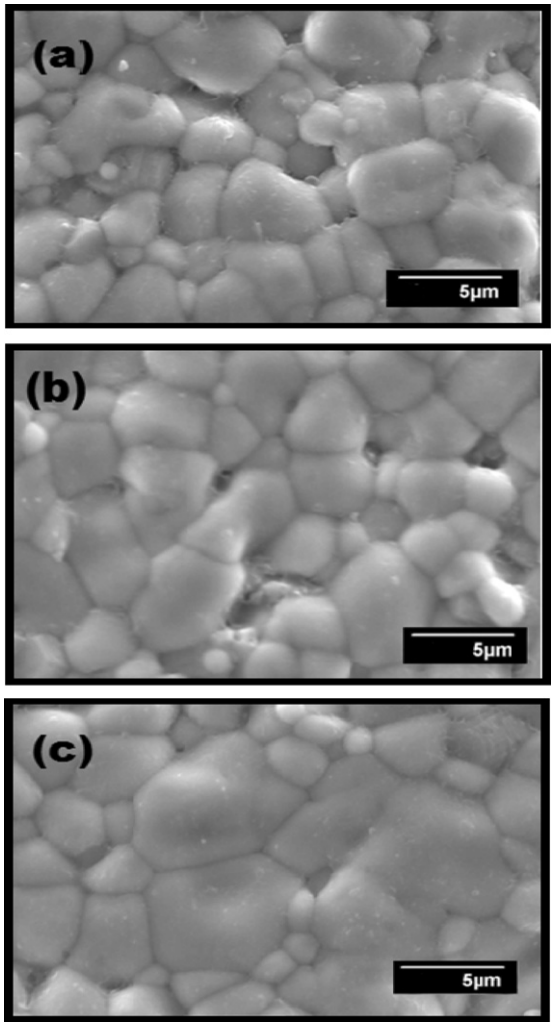

Fig. 3. (a and b) SEM micrograph of $CoFe_2O_4$ and $Co_{0.5}Zn_{0.5}Fe_2O_4$ samples. (c) SEM micrograph of $Co_{0.5}Mg_{0.5}Fe_2O_4$ sample.

3.2. Dielectric study

The variations of frequency dependence of real and imaginary part of dielectric permittivity at room temperature for $A_xCo_{1-x}Fe_2O_4$ (A = Zn, Mg and x = 0.0, 0.5) samples are shown in Fig. 4. It has been observed that all samples exhibit the dielectric dispersion where both real (ε') and imaginary part (ε'') decreases as the frequency increases from 1 Hz to 1 MHz. The dispersion behavior of $CoFe_2O_4$ and $Co_{0.5}Mg_{0.5}Fe_2O_4$ are clearly shown in inset of Fig. 4.

The measured data infers that in low frequency region the dielectric constant of $Co_{0.5}Zn_{0.5}Fe_2O_4$ is much higher than the $Co_{0.5}Mg_{0.5}Fe_2O_4$ and $CoFe_2O_4$. This difference is attributed to space charge polarization due to inhomogeneous dielectric structure. The inhomogeneties present in the structure may be the porosity, stoichiometry and grain structure. The space charges act as dipoles under the alternating electric field and hence contribute to the polarization. Also, there is chance of getting high dielectric constant because of large surface polarization owing to large surface area of individual grains. At lower frequency the grain boundary contribution are found to be more effective than the grain [17].

Moreover, the samples sintered at 1250 °C are highly dense as concluded by SEM measurements. Hence, stoichiometry and grain structure may be one of the reasons for higher dielectric constant of $Co_{0.5}Zn_{0.5}Fe_2O_4$ as compared to $Co_{0.5}Mg_{0.5}Fe_2O_4$ and $CoFe_2O_4$. But in the high frequency region, variation of dielectric constant is same for all the three samples. This is because at high region the contribution of dielectric constant mainly arises from electronic and ionic polarizations that are frequency independent.

Furthermore, the higher value of dielectric constant of $Co_{0.5}Zn_{0.5}Fe_2O_4$ may also be due to the fact that Zn ions might be evaporated from the surface layer due to high sintering temperature and as a result ferrous ions (Fe^{2+}) have been formed. Some of the Fe^{2+} ions have been transformed to Fe^{3+} ions during the sintering process and this generates free electrons, which contribute to the net polarization. The large number of electrons that are generated during transformation process will raise the dielectric constant of the sample. Similar kind of behavior is also observed in earlier reported data [5].

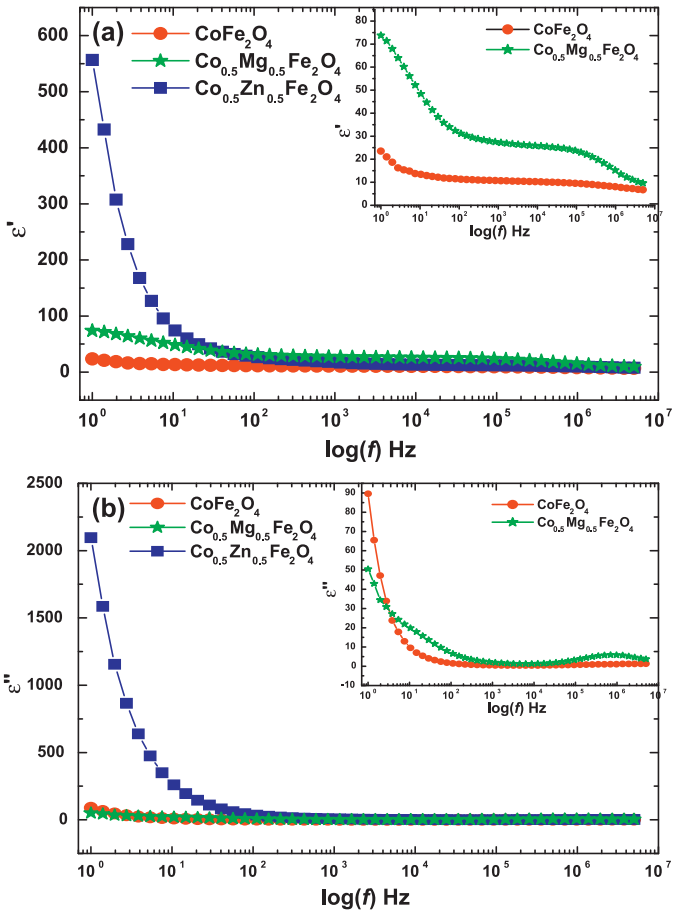

Fig. 4. Room temperature real permittivity (a) and imaginary permittivity (b) of $A_xCo_{1-x}Fe_2O_4$ (A = Zn, Mg and x = 0.0, 0.5) samples as a function of frequency.

According to Rabinkin et al., the mechanism responsible for polarization in ferrites is similar to that of conduction process [18]. The polarizations at lower frequencies are mainly attributed to electronic exchange between $Fe^{2+} \leftrightarrow Fe^{3+}$ ions on the octahedral site in the ferrite lattice. In present system a part from *n*-type charge carrier (Fe^{3+}/Fe^{2+}), the presence of (Co^{3+}/Co^{2+}) ions give rise to *p*-type charge carrier. Therefore in addition to *n*-type charge carrier, the local displacement of *p*-type charge carrier in direction of external electric field also contributes to net polarization. It has been observed that the dielectric constant decreases with increasing frequency and reaches a constant value due to the fact that beyond a certain critical frequency electron hoping cannot follow the alternating field. In view of the fact that mobility of *p*-type carrier is smaller than the *n*-type charge carrier, the contribution to polarization from former is smaller and decreases more rapidly even at lower frequencies than from the later. As a result the net polarization decreases with increase in frequency. Hence, the dielectric constant decreases.

Usually, the dielectric permittivity is described by:

$$C = \varepsilon_0 \varepsilon_r \frac{A}{d} \tag{2}$$

where C is the capacitance of the parallel plate capacitor with thickness d and area of cross section A, ε_0 is the permittivity of the free space (8.85×10^{-14} F cm) and ε_r is the relative permittivity of the dielectric medium in Eq. (2). As per earlier reported work, the dielectric dispersion in number of ferrite systems was explained satisfactory on the basis of Maxwell–Wagner theory of interfacial polarization in agreement with Koop's phenomenological theory [19]. According to this model, the dielectric medium is assumed to

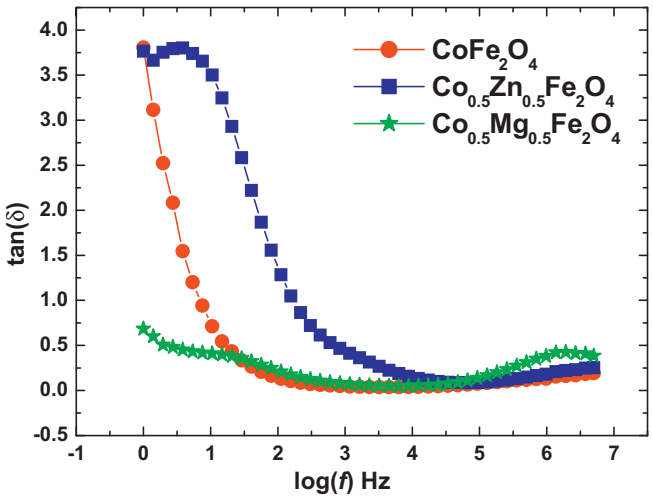

Fig. 5. Variation of loss tangent of $A_xCo_{1-x}Fe_2O_4$ (A = Zn, Mg and x = 0.0, 0.5) samples with variable frequency.

be made up of well conducting grains separated by poorly conducting grain boundaries. The grain boundaries are found to be more effective at lower frequencies while ferrite grains are more effective at higher frequencies. This normal dielectric behavior has been observed in many ferrites [20–23].

3.3. Loss tangent (tan δ)

The loss factor or the dissipation factor in any dielectric is represented as:

$$\tan\delta = \frac{\varepsilon''(\omega)}{\varepsilon'(\omega)} \quad \text{or} \quad \tan\delta = \frac{1}{2\pi f \varepsilon_0 \varepsilon' \rho} \tag{3}$$

Fig. 5 shows the variation of dielectric loss as a function of frequency for $A_xCo_{1-x}Fe_2O_4$ (A = Zn, Mg and x = 0.0, 0.5) samples. It has been observed that $Co_{0.5}Zn_{0.5}Fe_2O_4$ and $Co_{0.5}Mg_{0.5}Fe_2O_4$ samples exhibit a loss peak according to Debye relaxation theory. This loss peak occurs when the jumping frequency of electron between Fe^{2+} and Fe^{3+} is equal to the frequency of applied field and the condition $\omega\tau = 1 (\omega = 2\pi f)$ is satisfied. Similar kind of behavior is also observed in case of Mn—Zn ferrite [24]. The value of the loss tangent is minimum (~0.04) for $Co_{0.5}Zn_{0.5}Fe_2O_4$ and $Co_{0.5}Mg_{0.5}Fe_2O_4$ measured at a frequency of 5 kHz at room temperature comparable with earlier measured value of Mn—Zn ferrite [24,25]. Henceforth, $Co_{0.5}Zn_{0.5}Fe_2O_4$ and $Co_{0.5}Mg_{0.5}Fe_2O_4$ are suitable materials for microwave application because of low dielectric loss.

3.4. ac conductivity

In order to understand the conduction mechanism, the ac conductivity can be evaluated from the dielectric loss and dielectric permittivity and is represented by the relation:

$$\sigma_{ac} = \varepsilon' \varepsilon_0 \omega \tan\delta \tag{4}$$

The variation of ac conductivity of $A_xCo_{1-x}Fe_2O_4$ (A = Zn, Mg and x = 0.0, 0.5) samples as a function of frequency is represented in Fig. 6. The ac conductivity gradually increases as the frequency of applied field increases. At lower frequencies the grain boundaries are more effective than grains in electrical conduction hence the hopping of Fe^{2+} and Fe^{3+} ions are bound at lower frequencies. As the frequency of the applied field increases the conductive grains become more active and promote the conduction mechanism. It has been observed that in Co-ferrite there are two regions of conductivity, the low conductivity region containing Co^{2+} and Co^{3+} ions and

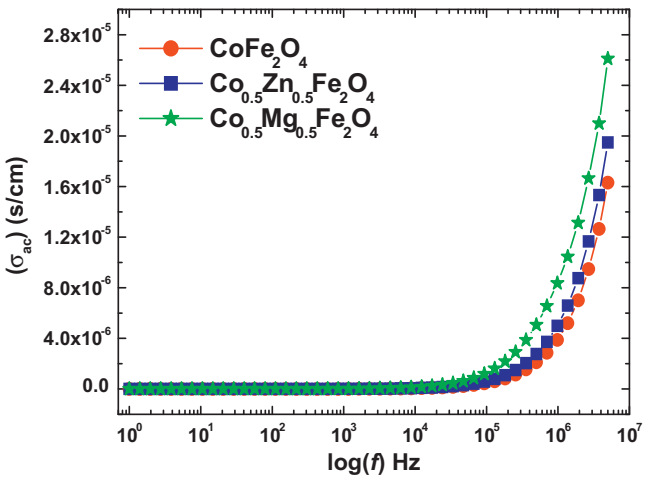

Fig. 6. Variation of ac conductivity for $A_xCo_{1-x}Fe_2O_4$ (A = Zn, Mg and x = 0.0, 0.5) samples with logarithmic frequency.

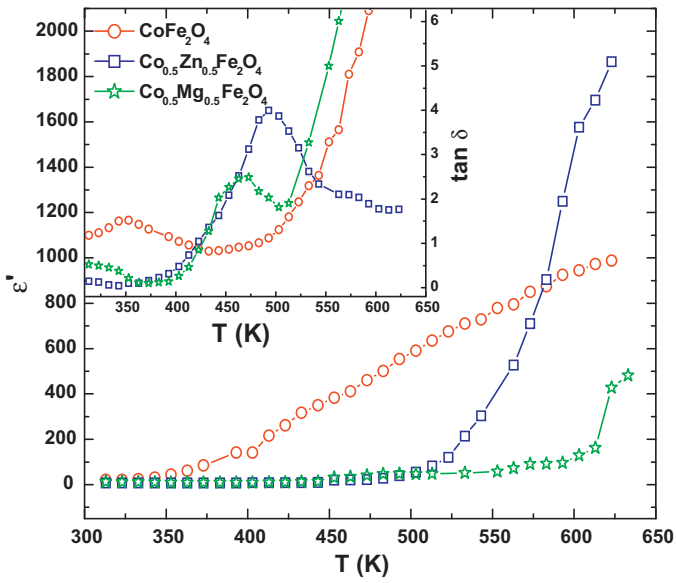

Fig. 7. The temperature dependence of the dielectric constant for $A_xCo_{1-x}Fe_2O_4$ (A = Zn, Mg and x = 0.0, 0.5) samples at 10 kHz. Inset shows the variation of loss tangent (tan δ) with temperature.

high conductivity region containing Fe^{2+} and Fe^{3+} ions [26]. The presence of Cobalt on octahedral site follows the charge exchange mechanism as:

$$Co^{2+} + Fe^{3+} \leftrightarrow Co^{3+} + Fe^{2+} \quad (5)$$

which predominantly explain the conduction mechanism in $CoFe_2O_4$. The conductivity of $Co_{0.5}Mg_{0.5}Fe_2O_4$ is high as compared to $Co_{0.5}Zn_{0.5}Fe_2O_4$ and $CoFe_2O_4$. This difference in the conductivities might be due to the difference in the grain size.

The conductivities of polycrystalline material decreases with decreasing grain size. Smaller grains imply large number of insulating grain boundaries and smaller grain-to-grain surface contact area, which act as a barrier to the flow of the electron [27]. The grain size of $CoFe_2O_4$ (3.2 μm) is smaller than $Co_{0.5}Zn_{0.5}Fe_2O_4$ (4.7 μm) and $Co_{0.5}Mg_{0.5}Fe_2O_4$ (7 4 μm). Hence conductivity is high for $Co_{0.5}Mg_{0.5}Fe_2O_4$, whereas, it is low for $Co_{0.5}Zn_{0.5}Fe_2O_4$, and for $CoFe_2O_4$ respectively.

Another factor that influences the electrical conductivity of the ferrites is the jump length (L) of the charge carrier. The hopping probability of the electron between the A (Fe^{3+})-site and B (Fe^{2+})-site are less as compared to the electrons that hop in between B (Fe^{2+})- and B (Fe^{2+})-sites. The reason being that the distance between the two metal ions placed at B-site is smaller than the distance if one is placed at A-site and other is at B-site. The L of the A and B sites is determined from the relation given as [28]:

$$L_A = a_0\left(\frac{\sqrt{3}}{4}\right) \quad (6a)$$

and

$$L_B = a_0\left(\frac{\sqrt{2}}{4}\right) \quad (6b)$$

The notations in Eq. (6) are the value of jump length as found to be L_A = 3.6178 Å, L_B = 2.9540 Å for $CoFe_2O_4$, L_A = 3.6165 Å, L_B = 2.9532 Å for $Co_{0.5}Zn_{0.5}Fe_2O_4$ and L_A = 3.6034 Å, L_B = 2.9421 Å for $Co_{0.5}Mg_{0.5}Fe_2O_4$. It has been observed that L decreases with Zn doping and further with Mg doping. The observed decrease in L suggests that charge carrier require less energy to jump from one cationic site to other, which causes an increase in conductivity. Hence the present result on the variation of ac conductivity with Zn^{2+} and Mg^{2+} doped ions shows that conductivity of $Co_{0.5}Mg_{0.5}Fe_2O_4$ is highest as compared to $Co_{0.5}Zn_{0.5}Fe_2O_4$ and $CoFe_2O_4$.

3.5. Temperature dependent ε' and tan δ

The temperature dependent dielectric constant and loss tangent of $A_xCo_{1-x}Fe_2O_4$ (A = Zn, Mg and x = 0.0, 0.5) samples are shown is shown in Fig. 7. It has been observed that both dielectric constant and loss tangent enhances with increase of temperature. This is attributed to the fact that hopping of charge carrier is thermally activated with increase of temperature causing the increase of dielectric polarization and henceforth both ε' and tan δ increases. The changes in the dielectric loss tangent (tan δ) with temperature at a frequency of 10 kHz represent a peaking behavior as shown in the inset of Fig. 7. The peak is attributed to the resonance effect arise due to the matching of the time period of the applied electric field with those of the corresponding relaxation phenomena.

The variation of relaxation time (τ) with temperature for $A_xCo_{1-x}Fe_2O_4$ (A = Zn, Mg and x = 0.0, 0.5) sample is illustrated in

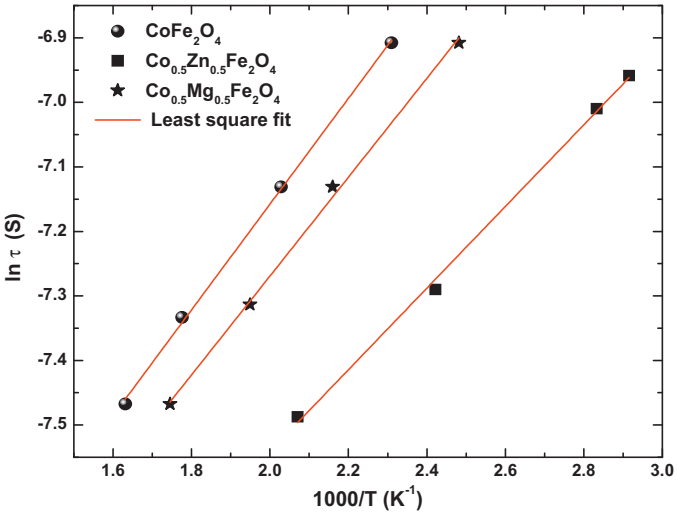

Fig. 8. The variation of dielectric relaxation time (τ) with temperature for $A_xCo_{1-x}Fe_2O_4$ (A = Zn, Mg and x = 0.0, 0.5) samples.

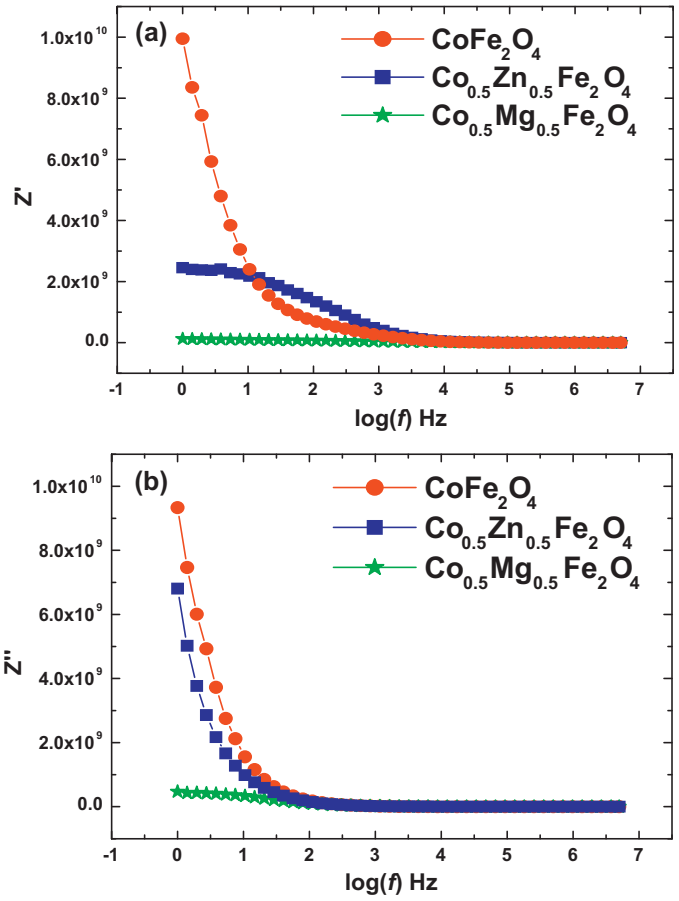

Fig. 9. Variation of real part of impedance spectra (a) and imaginary part of impedance spectra (b) with variable frequency of as synthesized samples.

Fig. 8. The above possess the temperature dependence of the relaxation time. We follow the Arrhenius law:

$$\tau = \tau_0 \exp\left(-\frac{E_a}{k_B T}\right) \quad (7)$$

where E_a is the activation energy of the relaxation process, k_B is the Boltzmann constant and τ_0 is the maximum relaxation time. It has been observed that the relaxation time decreases with the measuring temperature and is due to the thermal activated hopping frequency of electrons between Fe^{2+} and Fe^{3+} ions. The values of activation energy (E_a) obtained from the slope of the fitted curves are found to be 0.81 eV, 0.76 eV and 0.63 eV for $CoFe_2O_4$, $Co_{0.5}Mg_{0.5}Fe_2O_4$ and $Co_{0.5}Zn_{0.5}Fe_2O_4$ respectively. The activation energy decreases with the Mg and Zn dopant ions. This is in good agreement with the fact that lower activation energy is associated with higher dielectric constant and higher conductivity [29].

3.6. Impedance analysis

The impedance formalism helps in determining the interparticle interaction like grains, effect of grain boundaries *etc*. Fig. 9 represents the variation of real (resistive) and imaginary (reactive) part of impedance as a function of frequency for $A_xCo_{1-x}Fe_2O_4$ (A = Zn, Mg and x = 0.0, 0.5) samples. It is seen that impedance decreases as the frequency gradually increases. The maximum value of impedance is observed for $CoFe_2O_4$. In order to distinguish between the grain and grain boundary contribution the Nyquist plot of $A_xCo_{1-x}Fe_2O_4$ (A = Zn, Mg and x = 0.0, 0.5) samples were recorded at room temperature and are shown in Fig. 10. In general, the plot would be composed of three semicircles, depending upon the electrical properties of the material. The semicircle at lower frequency represents the sum of resistance of grains and grain boundaries, while the semicircle at higher frequency corresponds to the resistance of grains only [30]. The third semicircle is also observed in some materials, which could be due to the electrode effect [31,32]. In the present investigation, it has been observed that the impedance spectra of $CoFe_2O_4$ do not take the shape of the semicircle, but rather represent a straight line with large slope. This shows that grain boundary impedance is out of measurement scale, suggesting the insulating behavior of this composition. Whereas, for $Co_{0.5}Mg_{0.5}Fe_2O_4$ and $Co_{0.5}Zn_{0.5}Fe_2O_4$, the slope of the line decreases and curve towards the real (Z') axis.

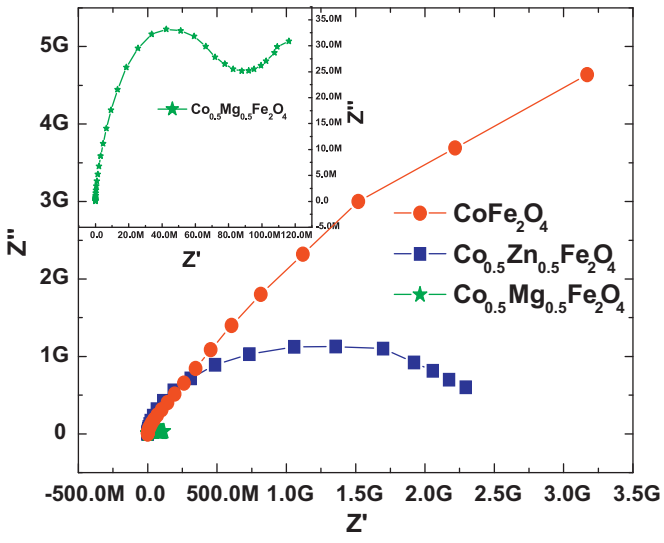

Fig. 10. Nyquist-plot of $A_xCo_{1-x}Fe_2O_4$ (A = Zn, Mg and x = 0.0, 0.5) samples.

For $Co_{0.5}Zn_{0.5}Fe_2O_4$ sample a flat semicircle is observed at higher frequency and is attributed to electrical conduction by the interior of the grain only, whereas, in case of $Co_{0.5}Mg_{0.5}Fe_2O_4$ (shown in the inset of Fig. 10) the impedance spectra represents two semicircular arcs. The intercept of semicircle with Z' at lower frequency represents the sum of resistance of grain and grain boundaries, while the intercept at higher frequency represents the resistance of grain only. The diameter of each semicircle corresponds to resistance of the grain [33]. The diameter of the semicircle changes with different doping elements. The diameter first reduces with substitution of Zn^{2+} ion and further with Mg^{2+} ions in $CoFe_2O_4$ indicating a change in grain interior resistance.

3.7. Modulus studies

The dielectric modulus is widely used to study the electrical relaxation in ionic and electronically conducting materials [11,34–36]. The variation of real and imaginary part of electrical modulus as a function of frequency is shown in Fig. 11. The observed values of stretched exponent parameter β for all the samples is less than unity and are found to be 0.86, 0.79, 0.68 for $CoFe_2O_4$, $Co_{0.5}Zn_{0.5}Fe_2O_4$ and $Co_{0.5}Mg_{0.5}Fe_2O_4$ respectively. The value of β helps to decide whether the relaxations present in the material is of Debye or non-Debye type. For an ideal dielectric for which the dipole–dipole interaction is negligible, the value of β is equal to unity. But the value of β is always less than unity for such a system in which the dipole–dipole interaction is significant. The observed values of stretched exponent parameter confirm the non-Debye type of dielectric relaxations.

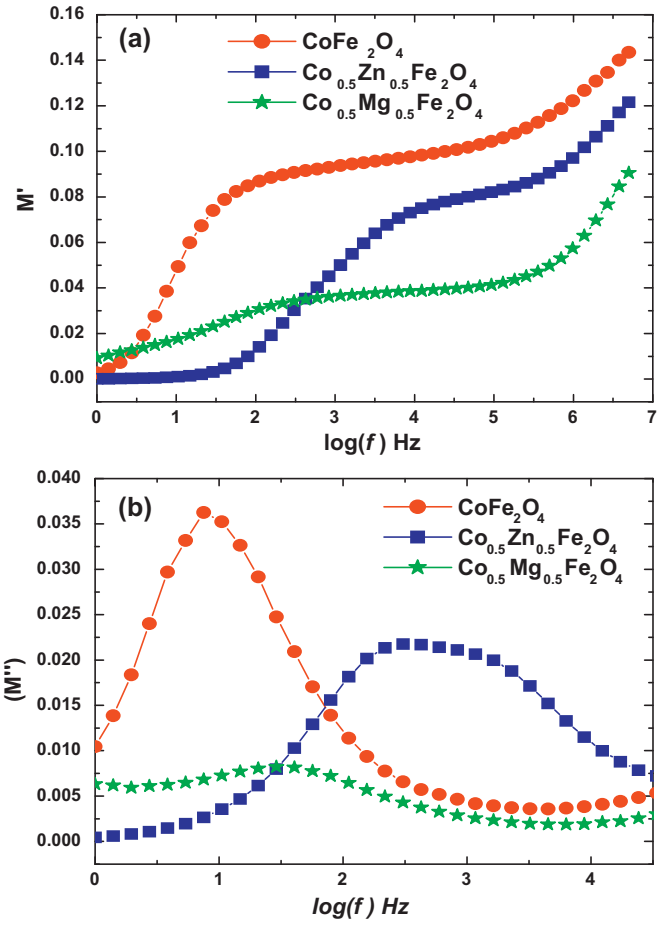

Fig. 11. Plot of real part of modulus (a) and imaginary part of modulus (b) spectra with respect to the frequency.

4. Conclusions

The samples of $A_xCo_{1-x}Fe_2O_4$ (A = Zn, Mg and $x = 0.0, 0.5$) were successfully prepared by chemical co-precipitation method. The effect of Zn and Mg doping on structural and dielectric properties of $CoFe_2O_4$ has been studied. X-ray powder diffraction confirms the formation of single-phase crystalline structure without any trace of impurity. All the samples fitted with Rietveld refinement using FULLPROF program revealed the existence of cubic structure (space group *Fd*3*m*). A slight reduction in the lattice parameter of $Co_{0.5}Mg_{0.5}Fe_2O_4$ has been observed as compared to pristine and $Co_{0.5}Zn_{0.5}Fe_2O_4$ ferrite.

The dielectric dispersion with frequency was observed and successfully explained on the basis of hopping mechanism. The lower value of dielectric loss for $Co_{0.5}Zn_{0.5}Fe_2O_4$ and $Co_{0.5}Mg_{0.5}Fe_2O_4$ makes them suitable material for microwave application. The observed ac conductivity is appropriate in the light of electron hopping between Fe^{2+} and Fe^{3+} ions. Temperature dependent dielectric constant and loss tangent of all the three samples shows an increasing trend with increasing temperature. However, the activation energy decreases with the substitution of Mg and Zn ions in parent $CoFe_2O_4$. The impedance spectra suggest a grain interior contribution in the conduction process. The electrical modulus study reveals the presence of non-Debye type of dielectric relaxation in the materials with the stretched exponent parameter β decreases with Zn and Mg doping.

Acknowledgments

Authors are thankful to Dr. Mukul Gupta, UGC-DAE CSR, Indore for caring out XRD measurement and Dr. M. Roy, MLS University, Udaipur for temperature dependent dielectric measurement. Financial assistance from UGC New Delhi is gratefully acknowledged. One of the authors (Kavita Verma) is gratefully acknowledged the RGNF UGC, New Delhi, India.

References

[1] B.D. Cullity, Introduction to Magnetic Materials, Addison-Wesley, New York, 1972.
[2] W.F.J. Fontijn, P.J. van der Zaag, M.A.C. Devillers, V.A.M. Brabers, R. Metselaar, Phys. Rev. B 56 (1997) 5432.
[3] N. Sivakumar, A. Narayanasamy, N. Ponpandian, G. Govindaraj, J. Appl. Phys. 101 (2007) 084116.
[4] J. Philip, P.D. Shima, B. Raj, Appl. Phys. Lett. 92 (2008) 043108.
[5] A. Verma, T.C. Goel, R.G. Mendiratta, M.I. Alam, Mater. Sci. Eng. B 60 (1999) 156.
[6] A. Dais, R.L. Moreira, J. Mater. Res. 13 (1998) 2190.
[7] M.R. Bhandare, H.V. Jamadar, A.T. Pathan, B.K. Chougule, A.M. Shaikh, J. Alloys Compd. 509 (2010) L113.
[8] N. Ponpandian, P. Balaya, A. Narayanasamy, J. Phys. Condens. Matter 14 (2002) 3221.
[9] A. Verma, D.C. Dube, J. Am. Ceram. Soc. 88 (2005) 519.
[10] T. Okamura, T. Fujimura, M. Date, Phys. Rev. 85 (1952) 1041.
[11] N. Ponpandian, A. Narayanasamy, J. Appl. Phys. 92 (2002) 2770.
[12] M.S. Khandekar, R.C. Kambale, J.Y. Patil, Y.D. Kolekar, S.S. Suryavanshi, J. Alloys Compd. 509 (2011) 1861.
[13] P. Kumar, S.K. Sharma, M. Knobel, M. Singh, J. Alloys Compd. 508 (2010) 115.
[14] P.A. Shaikh, R.C. Kambale, A.V. Rao, Y.D. Kolekar, J. Alloys Compd. 492 (2010) 590.
[15] I.H. Gul, A. Maqsood, M. Naeem, M. Naeem Ashiq, J. Alloys Compd. 507 (2010) 201.
[16] R.D. Shannon, Acta Cryst. A 32 (1976) 751.
[17] A.M. Abdeen, J. Magn. Magn. Mater. 192 (1999) 121.
[18] L.T. Rabinkin, Z.I. Novikova, Minsk: Acad. Nauk. USSR (1960) 146.
[19] C.G. Koop's, Phys. Rev. 83 (1951) 121.
[20] N. Singh, A. Agarwal, S. Sanghi, J. Alloys Compd. 509 (2011) 7543.
[21] D. Varshney, A. Kumar, K. Verma, J. Alloys Compd. 509 (2011) 8421.
[22] Mohd. Hashim, Alimuddin, S. Kumar, B.H. Koo, S.E. Shirsath, E.M. Mohammed, J. Shah, R.K. Kotnala, H.K. Choi, H. Chung, R. Kumar, J. Alloys Compd. 518 (2012) 11.
[23] Mohd. Hashim Alimuddin, S. Kumar, S. Ali, B.H. Koo, H. Chung, R. Kumar, J. Alloys Compd. 511 (2012) 107.
[24] N. Sivakumar, A. Narayanasamy, B. Jeyadevan, R.J. Joseyphus, C. Venkateswaran, J. Phys. D: Appl. Phys. 41 (2008) 245001.
[25] K. Latha, K.S. Mohan, D. Ravinder, Phys. Status Solidi A 142 (1994) K103.
[26] G.H. Jonker, J. Phys. Chem. Solids 9 (1959) 165.
[27] M. George, S.S. Nair, K.A. Malini, P.A. Joy, M.R. Anantharaman, J. Phys. D: Appl. Phys. 40 (2007) 1593.
[28] P.A. Shaikh, R.C. Kambale, A.V. Rao, Y.D. Kolekar, J. Alloys Compd. 482 (2009) 276.
[29] J. Smith, H.B.J. Wign, Ferrites, Cleaver-Hume Press, London, 1959.
[30] H. Inaba, J. Mater. Sci. 32 (1997) 1867.
[31] M.H. Abdullah, A.N. Yusuff, J. Mater. Sci. 32 (1997) 5817.
[32] N.V. Prasad, G. Prasad, T. Bhimasankaram, S.V. Suryanarayana, G.S. Kumar, Bull. Mater. Sci. 24 (2001) 487.
[33] H. Ye, R.B. Jackman, P. Hing, J. Appl. Phys. 94 (2003) 7878.
[34] A. Dias, R.L. Moreira, Mater. Lett. 39 (1999) 69.
[35] N. Baskaran, G. Govindaraj, A. Narayanasamy, Solid State Ionics 98 (1997) 217.
[36] P.B. Macedo, C.T. Moynihan, R. Bosech, Phys. Chem. Glasses 13 (1972) 171.